8-2008

# Image Properties in an Aberration-Corrected Photoemission Electron microscope

Rolf Könenkamp
*Portland State University*, rkoe@pdx.edu

T. Jones
*Portland State University*

J. Elstner
*Portland State University*

Robert Campbell Word
*Portland State University*, wordr@pdx.edu

Gertrude Rempfer
*Portland State University*

*See next page for additional authors*



## Citation Details

Könenkamp, R., Jones, T., Elstner, J., Word, R., Rempfer, G., Dixon, T., ... & Skoczylas, W. (2008). Image properties in an aberration-corrected photoemission electron microscope. Physics Procedia, 1(1), 505-511.

## Authors

Rolf Könenkamp, T. Jones, J. Elstner, Robert Campbell Word, Gertrude Rempfer, Todd Dixon, Luis Almaraz, and Walter P. Skoczylas

Available online at www.sciencedirect.com

ScienceDirect

Physics Procedia 1 (2008) 505–511

Physics Procedia

www.elsevier.com/locate/procedia

Proceedings of the Seventh International Conference on Charged Particle Optics

# Image properties in an aberration-corrected photoemission electron microscope

R. Könenkamp[a]*, T. Jones[a], J. Elstner[a], R.C. Word[a], G. Rempfer[a], T. Dixon[a], L. Almaraz[a], W. Skoczylas[b]

[a]*Physics Department, Portland State University, 1719 SW 10th Avenue, Portland, OR. 97201, U.S.A.*
[b]*FEI Company, Hillsboro, OR. 97124, U.S.A.*

Received 9 July 2008; received in revised form 9 July 2008; accepted 9 July 2008

**Abstract**

We report recent progress in the construction of a new aberration-corrected photoemission electron microscope. The correcting element in this instrument is a hyperbolic electron mirror which corrects for chromatic and spherical aberration. We present first images obtained with the new instrument and numerical results from trajectory and wave-optical calculations indicating that the resolution can be of the order of 1 nm. 

*PACS:* 68.37.Nq; 41.85.Gy; 79.69.-i

*Keywords:* Electron microscopy; Aberration correction; Photoemission

## 1. Introduction

Photoelectron emission microscopy (PEEM) has found numerous applications in surface science, magnetism, biology and other areas of science [1-8]. Its main advantage lies in a very high surface sensitivity that provides large contrast for surface topological features, for lateral changes in work-function, electron density and chemical structure. PEEM also minimizes electron exposure damage which makes it a method of choice in quality control applications and in soft matter studies. So far, however, the resolution of PEEM has remained at approximately 8 nm [9], which is inferior to scanning and transmission electron microscopy. This can in part be attributed to the large amount of aberration that occurs when the photo-emitted electrons are accelerated from the sample surface, where they have low kinetic energies, to typically a few tens of kV when they enter into the electron optical system. These aberrations add to the lens aberrations which are also present in SEMs and TEMs. In addition, since the field strength in the accelerating field in PEEM is limited by electrical breakdown, the objective lens in PEEM is usually operated at large focal lengths, which also results in increased spherical aberration. Finally, the acceleration process limits the aperture angle of the beam to values of only a few mrad, which contributes to a lowered resolution.

* Corresponding author. Tel.: +1-503-725-4224
*E-mail address*: rkoe@pdx.edu

doi:10.1016/j.phpro.2008.07.132

In this paper we discuss the resolution limits in an uncorrected and an aberration-corrected PEEM. Our calculations take into account the specific features of the mirror-corrected microscope that is in the final stage of construction in our lab. In the following we first briefly review the lay-out of this new instrument. We will then outline our approach of characterizing this system based on results from an experimental model system, numerical ray-tracing and a wave-optical analysis.

## 2. Description of our PEEM microscope

Fig. 1 shows a schematic diagram of the microscope. Different from the two synchrotron-based instruments under construction at Berkeley and in Berlin [10,11], our instrument is designed as a stand-alone instrument for near-uv photoexcitation. It has a Y-shaped beam-line to separate the beams incident on and exiting from a hyperbolic electrostatic mirror that serves as the correcting element. The deflection angles in the beam-line are approximately 20$^o$. It is noted that there are as many left-hand as right-hand deflections, and that the object, mirror and image planes have the same orientation. These features minimize deflection aberrations [12]. Fig. 2 shows the present status of the constructed instrument and a test image showing approximately 50 nm resolution.

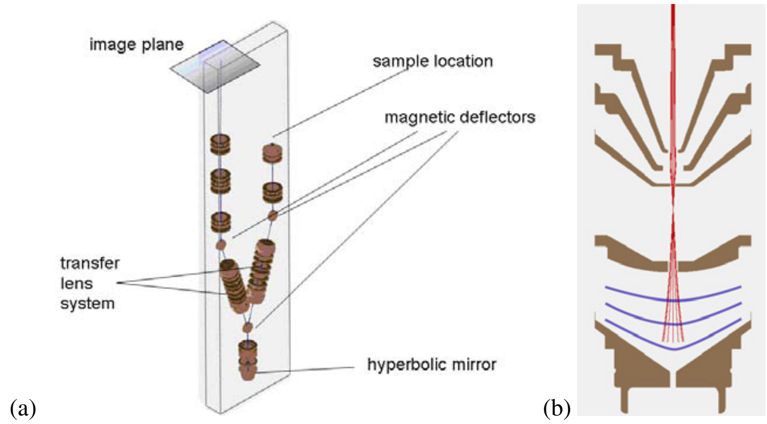


Fig. 1: (a) Schematic diagram of the beam-line I and lens arrangement in the aberration corrected microscope under construction at PSU. (b) Cross section of the hyperbolic mirror and mirror interface lens used as a correction-element for spherical and chromatic aberration. The mirror is operated in the symmetric mode, i.e. incident and exiting trajectories are along the same paths.

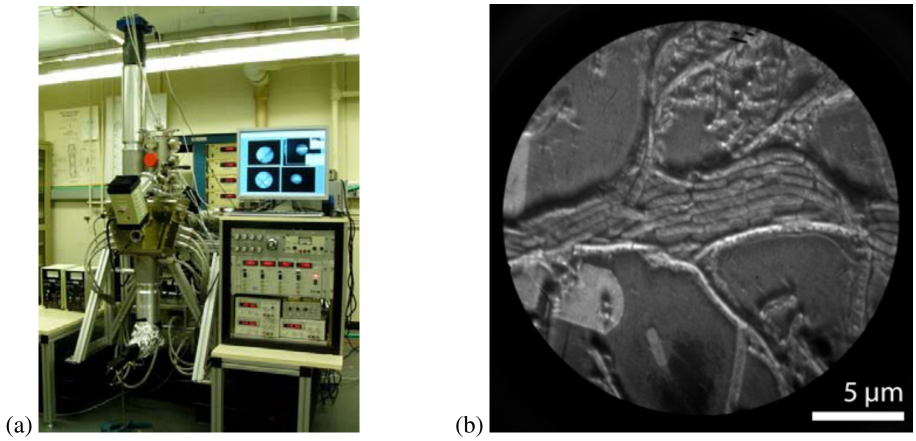


Fig. 2: (a) Present status of the constructed instrument. (b) Test image showing approximately 50 nm resolution.

Experimental work on a similar beam-line has been carried out by G. Rempfer earlier and demonstrated that this configuration is capable of compensating spherical and chromatic aberrations over a wide range of conditions [12,13]. The results indicate that the aberrations originating from the acceleration process can be compensated by the mirror arrangement. It was experimentally shown that the spherical and chromatic aberration coefficients, Cs and Cc, could be reduced to values of 1cm and 0.5 cm, respectively - a substantial reduction from values of Cs = 20 cm and Cc = 3.1 cm, obtained for a single uncorrected electrostatic lens [13]. In our PEEM a lens of this type is used as an objective lens with an accelerating gap of approximately 4 mm from the cathode. The focal length is about 10 mm. The acceleration process over the distance of 4 mm adds substantial amounts of spherical and chromatic aberrations, such that the overall values for the objective in a PEEM arrangement are typically Cs = 50 cm and Cc = 50 cm at a magnification of 15.

## 3. Numeric simulation with SIMION 7

To obtain accurate optical data specific to our system we have set up a numerical simulation of the constructed microscope using SIMION 7. At this point we have developed the simulation to a state that allows a trajectory calculation with high precision, and an individual characterization of all optical elements in the system. Eventually, however, we hope to obtain a precise analysis for the complete instrument. From the ray tracing analysis we will then be able to obtain the chromatic and spherical aberration coefficients for the whole instrument, compare these simulated results to the experimental findings, and in this fashion optimize the system.

## 4. Wave optical calculation of the Point Spread Function (PSF)

To obtain the limiting values for resolution, image signal intensity and contrast various instrument configurations we have developed a wave-optical approach that is capable of calculating the point spread functions in image space based on given values for Cs and Cc. As the SIMION work has not yet provided these we will use the experimental results previously obtained by G. Rempfer [13]. Four experimental configurations will be analyzed: a) an aberration-free lens system with Cs = 0 and Cc = 0; b) a typical objective lens with Cs = 20 cm and Cc = 3 cm as discussed in [13]; c) a typical objective system in a PEEM configuration including the acceleration aberrations with Cs = 50 cm and Cc = 50 cm.; d) an aberration-corrected lens system with Cs = 1 cm and Cc = 0.5 cm.

In the following we outline the wave-optical approach. The starting point in this characterization is the calculation of the wavefront shape in image space downstream from the last optical element in the microscope [14]. For a point source in an optical system with a given spherical aberration coefficient, Cs, the differential equation for the wavefront is given by

$$C_s\left(\frac{dz_w(y)}{dy}\right)^3 + \left(z_w(r) - z_o'\right)\frac{dz_w(r)}{dr} + r = 0 \qquad (1)$$

where the variables $r$ and $y$ are explained in Fig. 3. For small angles the solution to this equation can be approximated by,

$$z_u(y) = z_o' - \sqrt{z_o'^2 - y^2} + \frac{C_s}{4z_o'^4}y^4 \qquad (2)$$

From this wavefront equation we calculate numerically the phase distribution in an aperture plane located in field-free image space. Then a Fresnel integration is carried out to obtain the electron probability amplitude at a point i in the vicinity of the Gaussian image,

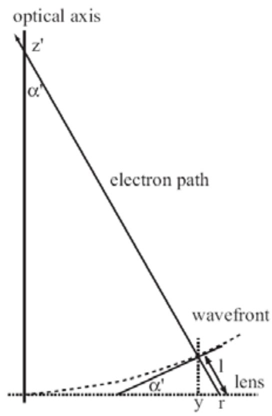

Fig. 3: Definition of the geometrical parameters used in eqs. (1) and (2).

$$\Psi(s,p) = \frac{i}{\lambda}\int_0^{2\pi}\int_0^{r_{ap}} r\Psi_0 e^{\varphi(r)} \frac{e^{i2\pi R(s,p,r,\Theta)/\lambda}}{R(s,p,r,\Theta)}\, dr\, d\Theta \qquad (3)$$

The point spread function (PSF) is then calculated from $\Psi^*\Psi$. For the results discussed here the location of the aperture plane was taken to be in the centre of the last lens. We have assumed that the initial energy of the photoelectrons is 1 eV as they exit the specimen, and that the energy gain in the acceleration field is 20 kV. This results in an object-side aperture of ~ 7 mrad. The calculation [15] is carried out in Mathematica 5.2. The oscillatory integrand in eq. (3) poses considerable problems for convergence, but a number of useful techniques have recently become available to obtain reliable results [16,17].

## 5. Computed results

Fig. 4 shows results from such a calculation for a single lens with an object distance of 3.9 cm, an image distance of 0.6 cm and a magnification of 0.154. These lens parameters correspond closely to those used in Rempfer's experimental work.

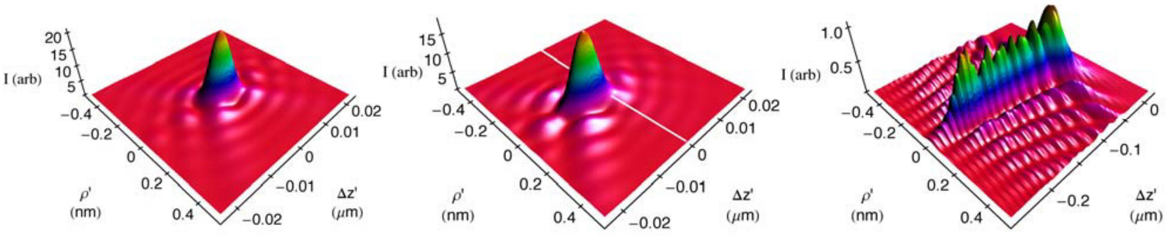


Fig. 4: Point spread functions. (a) For an ideal lens with Cs=0. (b) For an aberration-corrected lens with Cs=1cm. (c) For an uncorrected lens with Cs=20 cm.

Fig. 4(a) shows the PSF for an ideal lens with Cs = 0. The main maximum is centered on the Gaussian image point, but due to the small aperture value, the maximum is strongly elongated along the optical axis, giving a large depth of field. The first minimum in the radial direction occurs at 1.2 Å. From the Rayleigh criterion a point resolution of 8 Å is obtained by dividing by the magnification. This value is consistent with the formula R=0.61 λ / sinΘ. As the aperture angle of 7 mrad is set in the acceleration process, it cannot be optimized, and the obtained resolution value is the optimum for an aberration-free PEEM. The point-spread function shown in Fig. 4(b) is calculated for Cs = 1 cm which is the best value found in the experimental model system for the combination of an objective lens, auxiliary lenses and the mirror (13). This value is an estimated upper limit, set by the sensitivity of the used experimental technique. In Rempfer's work the aberration could smoothly be changed from positive to negative coefficients, but the experimental uncertainty for Cs was only 1 cm. The intensity maximum for this case is shifted from the Gaussian plane towards the lens, as expected for a positive aberration coefficient. The peak intensity is reduced by ~ 25% and the point resolution as obtained from the Rayleigh criterion is decreased by ~10%. Otherwise the PSF is qualitatively quite similar to the ideal PSF.

Fig. 4(c) shows a calculation for Cs = 20 cm - a typical value for a single electrostatic lens. The intensity is now widely spread in the radial and the longitudinal direction, the peak intensity is lowered by a factor 20, and the resolution is degraded by approximately 50% in comparison to the case in Fig. 3(a).

To incorporate chromatic aberration into the calculation we assume a Gaussian distribution of electron energies as indicated in Fig. 5(a), calculate the variation in image distance from the chromatic aberration coefficient, and then sum over the corresponding distribution of point spread functions. We assume an energy spread of 1 eV (FWHM) and typically sum over 200 energy values. The outcome is then normalized to the same total source brightness as used for all other calculations. Fig. 5(b) shows results from this calculation for the same lens as used in the context of Fig. 4. The radial intensity distributions shown are obtained in the plane of highest intensity, not the Gaussian image plane. The combination of Cs = 1 cm and a chromatic aberration coefficient of Cc = 0.1 cm results in an intensity reduction by a factor 3 and a marginal resolution impairment in comparison to the Cs = 0, Cc = 0 case. For Cs = 1cm and Cc = 3.1 cm, i.e. a spherically corrected, chromatically uncorrected lens the intensity and contrast loss are far more dramatic, emphasizing the importance of chromatic aberration correction for these lenses.

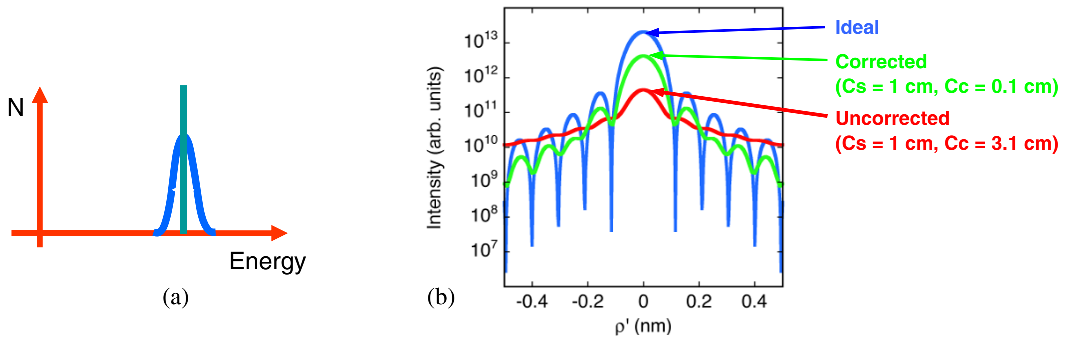


Fig. 5. (a) Energy distribution for the calculation of chromatic aberration effects with a standard width of 1 eV.
(b) Radial point-spread function in plane of highest intensity for various spherical and chromatic aberration coefficients obtained at M=0.154. The point resolution is obtained by dividing the radial distance for the first minimum by the magnification. This yields ~8 Å.

From the point spread functions, it is straightforward to calculate the optical transfer functions (OTF), which are the Fourier transforms (FT) of the PSF. We calculate the OTF by using a discrete Fourier transformation of the tabulated PSF. The OTF can be used to calculate the image properties also of extended objects by exploiting

FT (Image) = OTF . FT (Object).

The magnitude of the OTF, called the modulation transfer function (MTF), allows the resolution to be defined in more general terms than the Raleigh criterion (see, for example, Ref. [18]). The resolution from the Rayleigh criterion can be read from the MTF data by using a threshold value of 7% for the MTF amplitude. For large noise-levels in the image, however, a higher threshold value must be used [18]. In Fig. 6 we have plotted the MTF for the aberration-free objective lens, the uncorrected lens and the lens with a correction as obtained by Rempfer. It is noted that the aberration-corrected lens system with aberration coefficients, Cs = 1cm and Cc = 0.5 cm, will bring about considerable improvement, in comparison to a conventional uncorrected PEEM. Other results indicate that a combination of Cs = 1 cm and Cc = 0.1 cm will actually establish image properties very similar to the aberration-free case. With an aperture value of 7 mrad and a Gaussian energy spread of 1 eV, the point resolution in this case will be approximately 1 nm and the signal strength will be 30% of the aberration-free instrument.

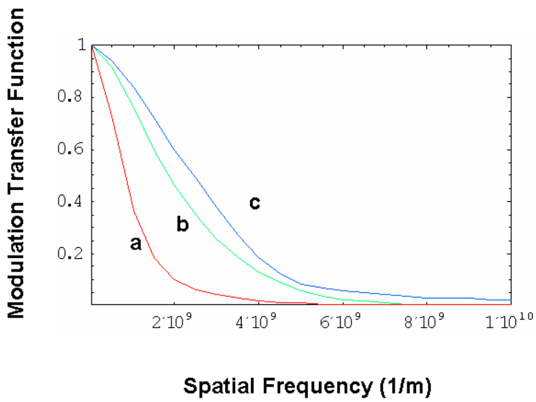

Fig. 6. Modulation transfer function for various values of the spherical and chromatic aberration coefficients. A useful estimate for the resolution can be obtained by requiring that the modulation amplitude be larger than the noise level. The 3 curves were calculated for different values of Cs and Cc. (a) Cs = 20 cm, Cc = 3.1 cm. (b) Cs = 1 cm, Cc = 0.5 cm. (c) Cs = 0 cm, Cc = 0 cm.

As a final consideration we include a plot of the PSF for a lens with Cs = 50 cm and Cc = 50 cm. These values constitute an estimate for a single uncorrected objective lens operated in the PEEM arrangement with initial electron energies of 0.25 eV and final energies of 30 kV [14]. Fig. 7 compares the point spread and modulation transfer functions for an uncorrected PEEM objective to the aberration-free case. The plots nicely demonstrate the gains in intensity that can be expected from aberration-correction in PEEM. The data indicate that the peak intensity in the image from the uncorrected PEEM objective is only ~ 0.3 % of the aberration-free case.

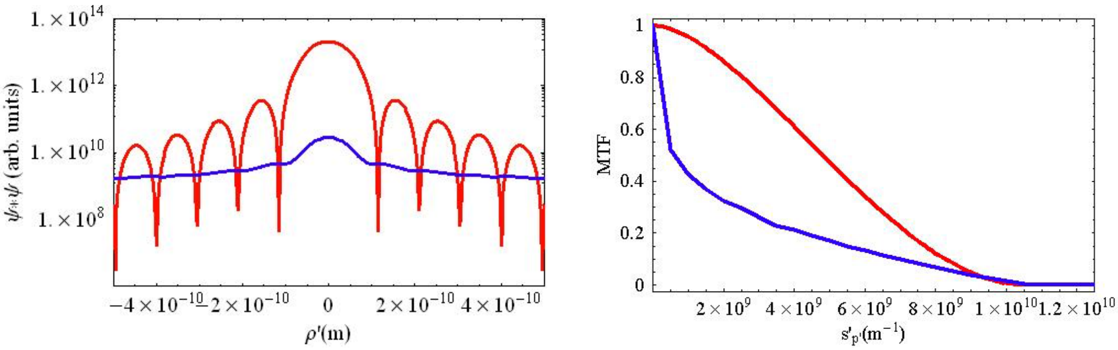


Fig. 7. (a) PSF for an ideal lens operated at 7 mrad object-side aperture and PSF of an uncorrected objective lens as operated in a PEEM, i.e. with an acceleration of electrons. Cs = 50 cm and Cc = 50cm are assumed for this lens. (b) MTF for an ideal lens operated at 7 mrad aperture and for a PEEM objective lens with Cs = 50 cm and Cc = 50 cm.

## 6. Conclusion

To conclude, we have presented calculations addressing the limitations in an aberration-corrected photoemission electron microscope. These results were obtained in an approach that is based on an experimental determination of aberration coefficients carried out earlier, and a wave-optical approach that includes chromatic and spherical aberration effects. Quantitative results for the resolution and the intensities have been obtained, and the point spread functions and the modulation transfer functions were calculated. Since the starting point for the calculations is the spherical aberration coefficient, the procedure allows a close comparison to experimental data obtained earlier. We find that mirror-based aberration-corrected instruments will be produce a significantly improved image quality as compared to conventional uncorrected instruments. In fact, aberration-correction will bring PEEMs into the same range as today's uncorrected SEMs.

## Acknowledgement

This work is partially supported by NSF under grant number DBI-0352224.

## References

[1] E. Bauer, J. Phys. Condensed Matter 13 (2001) 11391.
[2] S. Anders, H.A. Padmore, R.M. Duarte, T. Renner, T. Stammler, A. Scholl, M.R. Scheinfein, J. Stöhr, L. Se´ve and B. Sinkovic, Rev. Sci. Inst. 70 (1999) 3973.
[3] F. Nolting, A. Scholl, J. Stöhr, J. Fompeyrine, H. Siegwart, J.-P. Locquet, S. Anders, J. Lüning, E.E. Fullerton, M.F. Toney, M.R. Scheinfein, and H.A. Padmore, Nature 405 (2000) 767.

[4] F. Barbo, M. Bertolo, A. Bianco, G. Cautero, S. Fontana, T.K. Johal, S. La Rosa, R. C. Purandare, N. Svetchnikov, A. Franciosi, D. Orani, M. Piccin, S. Rubini and R. Cimino, Appl. Phys. Lett. 80 (2002) 2511.

[5] M. Cinchetti et al., Phys. Rev. Lett. 95 (2005) 047601.

[6] O.H. Griffith, D.L. Habliston, G.B. Birrell and W.P. Skoczylas, Biophys. J. 57 (1990).

[7] D.L. Habliston, G.B. Birrell, O.H. Griffith and G.F. Rempfer, J. Phys. Chem. 97 (1993) 3022.

[8] V. W. Ballarotto, K. Siegrist, R. J. Phaneuf, E. D. Williams, W.-C. Yang and R. J.Nemanich, Appl. Phys. Lett. 78 (2001) 3547.

[9] G. F. Rempfer and O. H. Griffith, Ultramicroscopy 27 (1989) 273.

[10] J. Feng, E. Forest, A. MacDowell, M. Marcus, H. Padmore, S. Raoux, D. Robin, A. Scholl and R. Schlueter, J. Phys. Condensed Matter 17 (2005) S1339.

[11] Th. Schmidt, U. Groh, R. Fink, E. Umbach, H. Marchetto, W. Engel, H.-J. Freund, P. Hartel, R. Spehr, H. Rose, G. Lilienkamp, E. Bauer, D. Preikszas and G. Benner, J. Vac. Sci. Technol. B 21 (2003).

[12] G. F. Rempfer, J. Appl. Phys. 67 (1990) 6027.

[13] G.F. Rempfer, D.M. Desloge, W.P. Skoczylas, and O.H. Griffith, Microscopy and Microanalysis 3 (1997) 14.

[14] J. Elstner, Thesis M.Sc. Physics, Portland State University (2004).

[15] T. Jones, Thesis M.Sc. Physics, Portland State University, to be published.

[16] S. Olver, Cambridge University, U.K., private communication.

[17] A. Iserles and S. Y, Norsett, Mathematics of Computation 75 (2006) 1233.

[18] M. Sato, “Resolution”, Chapter 8 in “Handbook of Charged Particle Optics”, J. Orloff ed., CRC Press, Boca Raton (1997).